Planetary and Space Science 157 (2018) 82–95

Contents lists available at ScienceDirect

Planetary and Space Science

journal homepage: www.elsevier.com/locate/pss

A spectroscopic survey of the small near-Earth asteroid population: Peculiar taxonomic distribution and phase reddening

D. Perna [a,b,*], M.A. Barucci [b], M. Fulchignoni [b], M. Popescu [b,c], I. Belskaya [b,d], S. Fornasier [b], A. Doressoundiram [b], C. Lantz [b,e], F. Merlin [b]

[a] INAF – Osservatorio Astronomico di Roma, Via Frascati 33, 00078 Monte Porzio Catone, Italy
[b] LESIA – Observatoire de Paris, PSL Research University, CNRS, Sorbonne Universités, UPMC Univ. Paris 06, Univ. Paris Diderot, Sorbonne Paris Cité, 5 Place Jules Janssen, 92195 Meudon, France
[c] Astronomical Institute of the Romanian Academy, 5 Cuţitul de Argint, 040557 Bucharest, Romania
[d] Institute of Astronomy, Kharkiv V.N. Karazin National University, Sumska Str. 35, Kharkiv 61022, Ukraine
[e] Institut d'Astrophysique Spatiale, CNRS, UMR-8617, Université Paris-Sud, bâtiment 121, 91405 Orsay, France

ARTICLE INFO

Keywords:
Techniques: spectroscopic
Minor planets
Asteroids: general
Near-Earth asteroids
Taxonomy
Phase reddening

ABSTRACT

We present the results of the first-ever visible spectroscopic survey fully dedicated to the small (absolute magnitude $H \geq 20$) near-Earth asteroid (NEA) population. Observations have been performed at the New Technology Telescope (NTT) of the European Southern Observatory (ESO), during a 30-night Guaranteed Time Observations programme, in the framework of the European Commission financed NEOShield-2 project. The visible spectra of 147 objects have been obtained and taxonomically classified. They show a peculiar taxonomic distribution, with respect to larger NEAs. In particular, olivine-rich A-types and organic-rich D-types are more abundant than what could be expected by extrapolating the taxonomic distribution of larger NEAs. Such results have implications for the investigation of the first phases of solar system history, including the delivery of prebiotic material on the early Earth. Having been obtained over a large range of solar phase angles, our data allowed us to evidence peculiar phase reddening behaviours for asteroids belonging to different taxonomic types. Low-albedo asteroids display no or limited phase reddening, compared to moderate- and high-albedo objects. This result suggests a promising novel way to distinguish primitive asteroids in the X-complex. In agreement with previous laboratory experiments, olivine-rich surfaces are the most affected by phase reddening.

1. Introduction

The investigation of near-Earth asteroids (NEAs) can provide crucial information on the formation and early evolution of the solar system, including topics like the delivery of water and organic-rich material to the early Earth, and the emergence of life (e.g., Marty et al., 2016). The reserve in water and rare metals held by NEAs is also getting the attention from government agencies and private companies, as asteroid mining could expand the Earth's resource bases in the near future (e.g., Sanchez and McInnes, 2013). Furthermore, NEAs represent a well-founded threat to human beings and life in general: the PHAs ("potentially hazardous asteroids") could in principle collide with the Earth within the next century and cause extensive damage (e.g., Perna et al., 2013, 2016).

The discovery rate of NEAs is constantly increasing and rapidly approaching the 2000 objects/year barrier. Current discoveries mainly concern "small" (tens/hundreds of metres in diameter) NEAs close approaching the Earth. The investigation of such small-sized NEAs is particularly important to constrain the asteroidal contribution to the delivery of prebiotic material (water and organic molecules) to our planet (e.g., Pierazzo and Chyba, 1999; Morbidelli et al., 2000; Saladino et al., 2013; O'Brien et al., 2014). Also in terms of the current impact risk, the small objects deserve our particular attention, as they have the highest statistical likelihood of impact, and can still produce a catastrophe at a regional/national scale (e.g., Perna et al., 2015a). More in general, the proximity of NEAs allows us to study asteroids about two to three orders of magnitude smaller than those observable in the main belt (i.e., down to metre-sized objects), hence to open new frontiers in asteroid science. Indeed, recent results already evidenced that small asteroids behave differently than the larger bodies in terms of rotational properties (Statler et al., 2013) and regolith generation (Delbo et al., 2014).

* Corresponding author. INAF – Osservatorio Astronomico di Roma, Via Frascati 33, 00078 Monte Porzio Catone, Italy.
E-mail addresses: davide.perna@oa-roma.inaf.it, davide.perna@obspm.fr (D. Perna).

https://doi.org/10.1016/j.pss.2018.03.008
Received 21 November 2017; Received in revised form 3 February 2018; Accepted 16 March 2018
Available online 17 March 2018

However, such small asteroids become bright enough to be physically characterized from Earth only for very limited time spans, coinciding with their close approaches with our planet, whereupon they could be unobservable for years or even for decades. Rapid-response physical observations of such bodies are hence necessary in order to not leave the characterization rate behind the discovery rate. In particular, visible and near-infrared photometry and reflectance spectroscopy of asteroids allow their taxonomic classification and provide clues about their surface composition, mineralogy and scattering properties. Such techniques can be "calibrated" via laboratory measurements on minerals and meteorites, as well as on the first returned samples from asteroids that we are getting in these years (e.g., DeMeo et al., 2015; Reddy et al., 2015). Currently, the fraction of NEAs with assigned taxonomic class (with respect to the known population in the same size range) drops from ~1/3 for km-sized bodies to ~1/10 for objects in the 0.3–1 km range, to ~1/100 for NEAs smaller than 300 m.

To soften this deficiency, in the framework of the NEOShield-2 project,[1] we performed the first-ever spectroscopic survey fully dedicated to the "small" NEAs, through a 30-night Guaranteed Time Observations programme at the 3.6-m New Technology Telescope of the European Southern Observatory (La Silla, Chile). The observational circumstances, as well as the data reduction and analysis are described in Section 2. In Section 3 we present our results, while Section 4 contains a discussion and our conclusions.

2. Methods

For our astronomical observations, the EFOSC2 spectrograph was used with the Grism #1 diffraction element. This configuration covers the spectral interval 0.40–0.92 μm with a resolution R~500 (~1.4 nm/pixel). Data were collected during twenty-four different nights spanning two years (April 2015 to March 2017), while six out of the thirty allocated nights were lost due to bad weather conditions. During each observing run, we gave preference to the smallest NEA observable (many of our targets were newly discovered bodies in proximity of their close approaches with the Earth), and limited our observations to objects with absolute magnitude equal or fainter than $H = 20$ (corresponding to a maximum diameter of about 300 m assuming a value of 0.20 for the visual albedo). On each observing night, we also observed several solar analogue stars. All of the spectra have been acquired through the 2 arcsec slit, oriented along the parallactic angle to minimize the effects of atmospheric differential refraction.

The data reduction followed standard procedures (e.g., Perna et al., 2015b): bias and background subtraction, flat-field correction, one-dimensional spectra extraction, atmospheric extinction correction. We used the Octave and IRAF software packages. Wavelength calibration was obtained using He-Ar lamps emission lines. The reflectance of the asteroids (normalized at 0.55 μm) was obtained by dividing their spectra by those of solar analogue stars observed close in time and in airmass to the scientific frames.

We taxonomically classified each object by performing curve matching with the visible part of the 25 template spectra defined by the Bus-DeMeo scheme (DeMeo et al., 2009), using the M4AST online tool (Popescu et al., 2012).

Overall, in this work we report the observations of 147 "small" NEAs. For all of them, Table 1 lists the asteroid number/designation, the absolute magnitude *H*, the observational circumstances (date and UT starting time, exposure time, airmass, and phase angle), as well as the solar analogue star used to obtain the reflectance spectrum (and the airmass at which the star was observed). The table also includes the spectral slopes and the associated errors computed using the Octave's *polyfit* routine (no further statistical/systematic potential sources of errors are considered in our analysis) in the 0.44–0.65 μm range (this wavelength interval was selected to roughly correspond to the B-R photometric colour, and to avoid both the silicate band and the lower signal-to-noise region longward of ~0.7 μm), as well as the result of the taxonomic classification, the considered albedo (cf. Table notes) and the computed equivalent diameter of each object. For NEA 2011 AM24 we found a quite odd spectral shape, not fitting any of the taxonomic types: while we tentatively classify this object as a potential D-type, we discard it from our following analysis. The distribution of the equivalent diameters of our targets is shown in Fig. 1. The spectra of 129 asteroids are presented in Fig. 2, while the remaining spectra of 18 objects classified as belonging to the D or A taxonomic types are presented and discussed in Perna et al. (2017; regarding D-type asteroid 1993 HA), Barucci et al. (2018; regarding further 9 D-types) and Popescu et al. (2018; regarding A-types).

3. Results

3.1. Taxonomic distribution

The taxonomic distribution of the observed NEAs is shown in Fig. 3. We report separate statistics for objects in the size bins 0–100 m and 100–300 m. Taking into account the uncertainties due to the availability of visible spectra only, to increase the significance of our analysis we group together objects belonging to the S-, C- and X-complexes. Moreover, we put in the X-complex the only target we classified as a T-type (with the objective of keeping well separated the primitive D-types from other featureless spectra in the X-complex). The distribution we found from our observations is dominated by the S-complex at all sizes, in agreement with previous results for larger NEAs. Such dominance is the consequence of both observational biases (albedo and phase angle effects) and preferential transport mechanisms from the inner asteroid main belt where S-type asteroids are dominant (e.g., Binzel et al., 2004). A proper debiasing of our observational results is beyond the scope of this paper, as it would be very much complicated by the still low statistics available for the small NEAs. We stress however that due to our constraint in the target selection concerning the absolute magnitude (only objects with $H \geq 20$ were considered), all of the larger objects (>300 m) in our sample are basically low-albedo ones. Conversely, one should remind of a bias against the discovery/observation of small low-albedo objects, which makes them very probably underrepresented in the 100–300 m and (especially) in the 0–100 m size ranges.

For comparison, Fig. 4 shows the distribution of taxonomic types in the literature, retrieved from the European Asteroid Research Node (EARN)[2] database of NEA physical properties. Taxonomic information for a total of 733 objects is reported, for different size bins (0–100 m, 100–300 m, 300–1000 m, >1 km). We use the same grouping criteria as in Fig. 3.

While the size distributions of our targets and of NEAs in the EARN database partly overlap, we can in first approximation consider them as representing "smaller" and "larger" asteroids, respectively. To compare statistically these two datasets in terms of taxonomic distribution, we used the following approach: (i) we randomly selected 146 objects from the EARN sample (i.e. the same number of NEAs characterized in our survey); (ii) we checked the taxonomic distribution of such random subsample; (iii) we repeated 10000 times steps (i) and (ii), and recorded the obtained mean and standard deviation for the population of each taxon. The results of such analysis are reported in Table 2. The most striking difference emerging when comparing our sample (i.e., "smaller" NEAs) with data reported in the literature (i.e., "larger" NEAs) concerns the overabundance of A- and D-types within the "small" NEA population, with deviations of about 5.6σ and 8.9σ with respect to the expected population of these taxa if the taxonomic distribution of NEAs in the EARN database could be assumed as the reference distribution. Being

[1] http://www.neoshield.eu/.

[2] http://earn.dlr.de; retrieved on 13 August 2017.

Table 1
Observational circumstances and data analysis results.

Object	H (mag)	Date/UT_{start}	t_{exp} (s)	Airmass	Solar analogue (airmass)	Phase angle (deg)	Slope (%/10^3 Å)	Taxon	Albedo	Equiv. Diam. (m)
4581 Asclepius	20.7	2015-6-8 6:02	3 × 1200	1.097	SA102-1081 (1.149)	18.8	6.163 ± 0.740	Cgh	0.065	378
52381 1993 HA	20.1	2015-11-5 6:41	2 × 450	1.06	HD11123 (1.021)	41.1	12.365 ± 0.338	D	0.140[(1)]	339
138852 2000 WN10	20.2	2015-11-6 8:15	2 × 450	1.091	HD9729 (1.089)	57.3	11.649 ± 0.267	Sq	0.243	246
162783 2000 YJ11	20.6	2015-7-19 2:19	1 × 1200	1.109	SA112-1333 (1.366)	17.7	16.642 ± 1.019	S	0.211	219
163348 2002 NN4	20	2016-8-29 0:49	2 × 1200	1.187	HD202282 (1.029)	44.5	3.151 ± 0.476	X	0.047	613
164202 2004 EW	20.7	2015-6-9 9:20	2 × 600	1.082	Hip106102 (1.051)	44	5.167 ± 0.526	X	0.340[(2)]	165
216523 2001 HY7	20.5	2015-4-14 9:41	2 × 600	1.176	SA112-1333 (1.260)	34.6	8.480 ± 1.057	Sq	0.243	214
281375 2008 JV19	20.7	2015-7-20 5:40	1 × 900	1.369	SA110-361 (1.176)	39.4	3.356 ± 0.578	C	0.050	431
293726 2007 RQ17	22.5	2015-6-8 7:44	2 × 600	1.288	SA107-998 (1.265)	50.7	40.851 ± 0.477	A	0.191	96
307070 2002 AV31	20.6	2017-1-3 7:54	2 × 1000	1.222	SA102-1081 (1.143)	33.8	5.899 ± 0.398	Xk	0.095	327
307564 2003 FQ6	20.8	2016-8-30 4:45	3 × 1200	1.084	HD202282 (1.038)	27.1	13.903 ± 0.236	S	0.211	200
326302 1998 VN	20.5	2016-11-29 8:07	1 × 800	1.145	HD33792 (1.191)	94.1	14.560 ± 0.688	V	0.362	175
330659 2008 GG2	22.8	2016-4-1 6:07	1 × 1100	1.05	HD171207 (1.030)	12.2	13.845 ± 1.567	Sq	0.243	74
334412 2002 EZ2	20.2	2016-4-1 4:48	2 × 700	1.224	HD106649 (1.039)	8.1	13.979 ± 0.336	S	0.400[(2)]	192
350713 2001 XP88	20.7	2015-7-19 8:10	2 × 900	1.191	SA115-271 (1.290)	15.4	7.062 ± 0.303	Xc	0.129	268
388945 2008 TZ3	20.4	2016-4-1 6:25	2 × 600	1.343	SA107-998 (1.358)	25.6	4.250 ± 0.285	C	0.050	494
401885 2001 RV17	20.4	2015-11-6 1:40	2 × 1100	1.244	SA112-1333 (1.260)	84.2	15.737 ± 0.480	Sv	0.309	199
410777 2009 FD	22.1	2015-11-7 0:39	2 × 900	1.53	HD9729 (1.452)	39.7	4.326 ± 0.257	X	0.010[(3)]	505
418849 2008 WM64	20.7	2015-12-14 7:11	1 × 900	1.415	SA98-978 (1.371)	73.8	18.279 ± 0.376	Sa	0.367	159
420262 2011 KD11	20.1	2015-6-9 0:31	2 × 1050	1.024	SA102-1081 (1.556)	30.4	18.345 ± 0.636	D	0.048	579
420738 2012 TS	20.8	2015-11-6 5:42	2 × 900	1.037	HD36649 (1.125)	51.6	7.763 ± 0.345	X	0.047	424
433953 1997 XR2	20.8	2017-1-2 3:00	2 × 630	1.209	SA102-1081 (1.142)	31	8.701 ± 0.314	Xe	0.136	249
438955 2010 LN14	21.1	2015-6-8 9:02	2 × 600	1.065	SA102-1081 (1.149)	35.5	7.418 ± 0.262	Q	0.227	168
441987 2010 NY65	21.5	2015-7-19 1:14	2 × 1200	1.226	SA107-998 (1.269)	46	19.824 ± 0.491	Sv	0.071[(4)]	250
444584 2006 UK	20.2	2016-5-12 6:28	1 × 600	1.731	SA107-998 (1.313)	29.2	25.838 ± 0.961	A	0.191	277
446924 2002 VV17	20.1	2015-11-6 6:12	2 × 300	1.454	SA98-978 (1.144)	14.1	9.537 ± 0.256	Q	0.227	266
447221 2005 UO5	20.7	2015-11-6 3:54	2 × 750	1.087	HD9729 (1.089)	43.8	8.022 ± 0.519	Q	0.227	202
452302 1995 YR1	20.3	2015-12-14 6:49	1 × 600	1.347	SA98-978 (1.371)	35.3	7.315 ± 0.256	Xk	0.095	376
455659 2005 BO1	21.6	2015-12-15 4:40	1 × 900	1.111	SA98-978 (1.145)	28	9.782 ± 0.848	Q	0.227	134
457663 2009 DN1	20.3	2016-7-1 8:09	2 × 1200	1.196	SA102-1081 (1.278)	55.5	3.041 ± 0.598	X	0.047	534
458135 2010 GE25	20.2	2016-3-30 1:54	1 × 1200	1.256	SA102-1081 (1.297)	62.4	11.218 ± 0.928	Sv	0.230[(4)]	253
462559 2009 DD1	20.4	2016-8-30 1:32	2 × 1200	1.231	SA110-361 (1.229)	46.4	10.121 ± 0.655	Xe	0.136	300
466507 2014 FK33	20.8	2016-4-1 7:13	2 × 850	1.135	HD171207 (1.030)	13.2	12.714 ± 0.808	Sq	0.243	187
467352 2003 KZ18	21.3	2015-6-9 2:40	2 × 900	1.065	Hip56139 (1.030)	32.4	9.050 ± 0.465	D	0.048	333
468005 2012 XD112	21.2	2015-12-14 2:24	1 × 1200	1.325	SA98-978 (1.371)	24.8	9.373 ± 0.702	Sq	0.243	155
468681 2009 MZ6	20.5	2016-7-1 5:23	1 × 1200	1.228	SA102-1081 (1.278)	19.8	7.768 ± 1.005	Q	0.227	222
468741 2010 VM1	20.1	2016-7-1 7:13	2 × 1200	1.326	HD206938 (1.240)	42.3	11.777 ± 0.364	Q	0.227	266

(*continued on next page*)

Table 1 (*continued*)

Object	H (mag)	Date/UT_{start}	t_{exp} (s)	Airmass	Solar analogue (airmass)	Phase angle (deg)	Slope (%/10^3 Å)	Taxon	Albedo	Equiv. Diam. (m)
469737 2005 NW44	20.4	2016-6-30 8:31	1 × 900	1.094	HD146997 (1.240)	49.3	8.502 ± 0.724	Xe	0.136	300
470864 2008 YV148	20.5	2016-6-30 7:18	2 × 1800	1.022	HD220764 (1.045)	25.9	10.146 ± 1.463	Sq	0.243	214
471240 2011 BT15	21.7	2016-9-1 9:18	4 × 600	1.284	SA93-101 (1.179)	32.5	16.742 ± 0.206	Sr	0.266	118
474163 1999 SO5	20.9	2016-11-29 3:20	2 × 1200	1.083	HD6400 (1.075)	52.2	19.833 ± 0.571	Sv	0.309	158
480823 1998 YW5	20	2016-11-30 7:01	1 × 1800	1.224	HD20926 (1.389)	35.4	14.187 ± 0.763	Sv	0.309	239
480922 2002 XP37	20.4	2017-1-2 1:54	2 × 750	1.179	HD16640 (1.335)	54.4	12.462 ± 0.298	Q	0.227	232
482566 2012 WK4	21.5	2016-11-29 5:35	2 × 1188	1.211	HD30947 (1.239)	15.3	18.135 ± 0.515	R	0.148	173
2002 RB	20.9	2015-7-19 6:26	2 × 1200	1.048	HD2966 (1.065)	19.1	−1.112 ± 0.351	Cb	0.043	423
2005 ML13	22.5	2017-1-3 6:54	2 × 1200	1.574	SA98-978 (1.528)	27.8	14.360 ± 0.583	S	0.211	91
2005 PH2	20.4	2016-3-30 7:49	1 × 840	1.305	SA107-998 (1.264)	31.1	−0.046 ± 1.302	C	0.050	494
2005 XT77	21.1	2015-11-6 7:19	1 × 1200	1.107	HD9729 (1.089)	66.6	10.724 ± 1.110	Sq	0.243	162
2007 VM184	21	2016-11-29 0:50	2 × 240	1.375	SA115-271 (1.218)	29.7	13.557 ± 0.264	S	0.211	183
2007 WQ3	21.2	2015-11-5 2:16	3 × 1200	1.238	Hyades64 (1.439)	18.2	11.935 ± 0.411	Sq	0.243	155
2007 WU3	23.8	2015-7-20 1:16	3 × 1200	1.185	SA110-361 (1.176)	35.7	5.116 ± 0.779	X	0.047	107
2008 CA6	20.5	2017-2-28 3:53	3 × 300	1.048	HD94093 (1.059)	33.9	12.609 ± 0.230	Sr	0.266	205
2008 CS1	20.1	2016-8-31 0:09	2 × 1200	1.105	HD202282 (1.032)	57.8	13.471 ± 0.321	Sq	0.243	257
2008 GU20	23.1	2016-4-1 2:12	3 × 1500	1.104	SA98-978 (1.187)	25.4	14.070 ± 0.579	S	0.211	69
2009 CV	24.3	2016-6-29 0:26	1 × 800	1.031	Hip52311 (1.199)	48.8	9.968 ± 0.620	D	0.048	84
2009 DL46	22	2016-6-30 4:03	2 × 1200	1.243	HD146997 (1.240)	35.9	9.106 ± 0.837	D	0.048	241
2009 EM1	23	2017-3-1 7:40	1 × 1800	1.522	HD113171 (1.544)	18.7	13.817 ± 1.028	Sq	0.243	68
2009 MW	20.8	30/06/16 01:31	2 × 600	1.027	HD147034 (1.036)	29.7	13.016 ± 0.353	Sq	0.243	187
2011 AM24	20.4	2015-6-8 2:27	1 × 1350	1.732	SA107-998 (1.265)	49.8	32.067 ± 0.833	D?	0.2?	247?
2011 OL5	20.2	2015-6-8 7:04	2 × 750	1.493	SA110-361 (1.274)	36.7	11.399 ± 0.435	Xe	0.136	329
2012 DR32	24.8	2017-2-28 6:02	2 × 400	1.619	HD88749 (1.188)	26.7	4.281 ± 0.301	Xc	0.129	41
2012 NP	21.3	2015-7-20 2:17	2 × 900	1.356	HD111244 (1.060)	40.7	30.543 ± 0.527	A	0.191	167
2012 PG6	20.3	2015-7-19 7:10	2 × 900	1.05	HD2966 (1.065)	14.1	5.245 ± 0.871	X	0.047	534
2012 RS16	21.4	2015-7-19 23:45	2 × 1200	1.329	SA107-998 (1.233)	35	24.760 ± 1.004	V	0.362	116
2012 XA133	21	2015-12-15 1:34	2 × 900	1.228	Hip9329 (1.043)	44	6.494 ± 1.440	Q	0.227	176
2013 YE38	20.1	2016-11-30 8:19	1 × 900	1.098	HD20926 (1.062)	57.3	10.396 ± 0.309	D	0.048	579
2014 GF50	20.7	2016-8-31 2:12	3 × 1200	1.059	SA110-361 (1.149)	34.6	18.374 ± 0.437	Sq	0.243	195
2014 OE338	21	2015-7-20 4:45	2 × 1200	1.272	SA110-361 (1.176)	22.7	7.503 ± 1.108	Xc	0.129	233
2014 QK362	21.6	2015-7-19 4:22	3 × 900	1.008	SA112-1333 (1.366)	1.6	1.217 ± 0.524	Cb	0.043	307
2014 TF17	20.8	2015-4-14 8:33	2 × 600	1.235	SA102-1081 (1.202)	32.8	4.129 ± 1.075	X	0.047	424
2014 WP365	20.2	2015-4-14 2:59	1 × 300	1.089	SA102-1081 (1.202)	48.9	11.783 ± 1.244	S	0.211	264
2014 YC	22.2	2017-1-2 3:48	1 × 1333	1.087	SA102-1081 (1.142)	32.1	6.973 ± 0.824	Xc	0.129	134
2014 YS34	20.8	2015-6-9 7:14	2 × 1125	1.249	SA102-1081 (1.556)	20.1	24.958 ± 0.978	A	0.191	210
2015 AY245	21.1	2015-7-20 3:27	3 × 1200	1.369	HD154424 (1.234)	32.4	6.690 ± 0.674	T	0.042	391
2015 BY310	21.7	2015-6-8 9:44	2 × 1200	1.11	SA102-1081 (1.149)	44.5	12.418 ± 0.954	Sr	0.266	118

(*continued on next page*)

Table 1 (*continued*)

Object	H (mag)	Date/UT_{start}	t_{exp} (s)	Airmass	Solar analogue (airmass)	Phase angle (deg)	Slope (%/10^3 Å)	Taxon	Albedo	Equiv. Diam. (m)
2015 DR215	20.5	2016-4-1 0:29	2 × 900	1.624	SA107-998 (1.353)	92.1	17.527 ± 1.265	Sr	0.266	205
2015 FD134	20.4	2015-6-9 2:06	1 × 1200	1.189	SA102-1081 (1.556)	48.6	17.291 ± 0.904	Sv	0.309	199
2015 GF	20.9	2015-6-8 8:28	2 × 900	1.172	SA115-271 (1.185)	27.6	16.096 ± 0.557	Sr	0.266	170
2015 HA1	21.2	2015-6-9 1:09	1 × 1200	1.441	SA102-1081 (1.556)	82.3	13.890 ± 0.533	L	0.149	198
2015 HB117	23.6	2015-6-8 4:24	2 × 1200	1.359	SA102-1081 (1.149)	33	26.095 ± 0.979	A	0.191	58
2015 HM10	23.6	2015-7-20 8:10	2 × 1200	1.26	HD111244 (1.060)	63.4	18.302 ± 1.068	R	0.148	66
2015 HP43	21.1	2015-6-8 3:00	1 × 900	1.047	SA115-271 (1.185)	23	8.330 ± 0.556	Q	0.227	168
2015 JD1	20.7	2015-11-7 8:51	3 × 400	1.114	HD625558 (1.102)	63.7	16.824 ± 1.502	L	0.149	249
2015 JJ2	21.9	2015-6-9 4:45	1 × 900	1.111	SA110-361 (1.151)	16.8	2.919 ± 0.757	C	0.050	248
2015 JY1	20.8	2015-6-8 0:16	2 × 750	1.003	SA102-1081 (1.149)	47	15.732 ± 0.289	R	0.148	239
2015 KS121	22.8	2015-6-9 5:50	1 × 600	1.139	SA107-998 (1.149)	10.9	3.075 ± 1.473	X	0.047	169
2015 KU121	22.9	2015-6-7 23:25	1 × 150	1.117	SA102-1081 (1.149)	80.1	12.465 ± 0.615	Q	0.227	73
2015 LH	27.3	2015-6-9 6:30	1 × 180	1.426	SA102-1081 (1.556)	43.5	37.935 ± 1.700	A	0.191	11
2015 LH14	20.1	2015-7-19 0:35	1 × 900	1.383	SA107-998 (1.269)	41	11.873 ± 0.454	Xc	0.129	353
2015 LN21	23	2015-7-1 9:22	2 × 1200	1.425	SA115-271 (1.290)	54.1	19.597 ± 0.680	D	0.048	152
2015 LU24	20.4	2015-7-20 6:35	2 × 1200	1.391	SA110-361 (1.176)	57.2	19.405 ± 1.047	Sa	0.367	182
2015 MN44	22.5	2015-7-19 5:26	3 × 1200	1.042	HD2966 (1.065)	9.9	7.278 ± 0.518	Q	0.227	88
2015 QQ3	21.3	2015-11-5 4:34	3 × 1200	1.058	HD9729 (1.052)	30.7	8.524 ± 0.519	Sq	0.243	148
2015 RD37	20.1	2015-11-5 3:19	2 × 600	1.032	HD11123 (1.021)	25.1	15.448 ± 0.452	V	0.362	211
2015 RG36	20.3	2015-11-6 0:48	2 × 1100	1.046	HD9729 (1.089)	56.6	11.329 ± 0.430	S	0.211	252
2015 TA	21.6	2015-11-7 1:37	2 × 1800	1.046	HD7186 (1.040)	50.6	16.424 ± 0.901	S	0.211	138
2015 TA25	20.1	2015-11-7 3:28	2 × 600	1.655	HD9729 (1.452)	11.7	11.422 ± 0.250	S	0.211	276
2015 TB179	20.6	2015-11-5 7:34	3 × 1200	1.203	HD11123 (1.021)	27.1	25.344 ± 0.713	A	0.191	231
2015 TG238	22.8	2015-11-7 2:49	2 × 1200	1.181	HD9729 (1.452)	15.4	2.841 ± 0.982	X	0.047	169
2015 TJ1	22.7	2016-3-31 2:53	1 × 1200	1.077	SA102-1081 (1.288)	37.8	1.142 ± 0.833	Cb	0.043	185
2015 TK238	21.9	2015-11-6 4:44	1 × 1200	1.168	SA112-1333 (1.260)	17.8	7.063 ± 0.611	Q	0.227	116
2015 TL143	23.3	2015-11-6 3:15	2 × 900	1.051	SA112-1333 (1.260)	55.8	13.618 ± 0.360	Sv	0.309	52
2015 TM143	23.6	2015-11-6 2:29	2 × 1200	1.13	HD3011 (1.120)	69.2	−0.348 ± 0.596	Cb	0.043	122
2015 TW144	20.7	2015-11-5 5:46	2 × 900	1.285	Hyades64 (1.439)	21.5	27.093 ± 0.531	A	0.191	220
2015 TY144	21.4	2015-11-6 7:48	1 × 1200	1.132	HD9729 (1.089)	33.7	11.559 ± 0.715	Q	0.227	146
2015 TZ237	24.3	2015-11-7 4:13	2 × 1200	1.571	HD9729 (1.452)	4.9	6.030 ± 0.577	X	0.047	85
2015 UC	24.8	2015-11-7 5:02	2 × 1200	1.183	HD9729 (1.452)	13.8	11.450 ± 0.326	Sq	0.243	30
2015 UJ51	21.5	2015-11-7 5:53	2 × 1200	1.244	HD625558 (1.102)	12.6	6.906 ± 0.503	Q	0.227	140
2015 UK52	20.1	2015-12-14 1:29	1 × 900	1.194	SA93-101 (1.152)	77.2	13.185 ± 0.451	Sr	0.266	246
2015 UT52	20.9	2015-12-14 3:30	1 × 600	1.453	Hyades64 (1.455)	7.2	4.536 ± 0.333	X	0.047	405
2015 WG9	20.3	2015-12-15 3:16	3 × 900	1.139	HD2966 (1.101)	35.8	6.396 ± 1.029	Sq	0.243	235
2015 XE	24.6	2015-12-14 5:48	2 × 900	1.368	HD2966 (1.079)	17.3	7.894 ± 0.367	K	0.130	44

(*continued on next page*)

Table 1 (*continued*)

Object	H (mag)	Date/UT_{start}	t_{exp} (s)	Airmass	Solar analogue (airmass)	Phase angle (deg)	Slope (%/10^3 Å)	Taxon	Albedo	Equiv. Diam. (m)
2015 XK1	20	2015-12-14 4:36	2 × 600	1.197	HD2966 (1.079)	27.8	9.671 ± 0.326	Q	0.227	279
2016 CB30	23.6	2016-3-30 4:29	3 × 800	1.162	SA102-1081 (1.297)	11.9	0.105 ± 0.447	Cb	0.043	122
2016 CZ135	20.7	2016-11-30 2:00	1 × 1500	1.113	HD4941*1.097	27.6	13.672 ± 0.638	Sv	0.309	173
2016 EC157	23.5	2016-4-1 3:28	2 × 1800	1.163	SA98-978 (1.187)	15.6	11.396 ± 0.738	S	0.211	58
2016 EK27	22.3	2016-4-1 5:21	1 × 750	1.01	HD106649 (1.010)	31	11.306 ± 0.462	S	0.211	100
2016 LM1	20	2016-7-1 9:38	2 × 1200	1.019	HD3011 (1.009)	61.2	13.535 ± 0.697	L	0.149	344
2016 LU10	20.9	2016-9-1 8:02	3 × 1200	1.159	HD202282 (1.032)	32	2.471 ± 0.313	C	0.050	393
2016 LZ10	20	2016-7-1 4:37	3 × 900	1.175	HD125910 (1.071)	21	3.027 ± 0.466	B	0.120	384
2016 MF1	20.9	2016-8-30 2:50	1 × 1200	1.074	HD202282 (1.038)	9.4	6.299 ± 0.507	O	0.339	151
2016 OJ1	21.7	2016-8-29 7:42	1 × 1200	1.019	SA93-101 (1.181)	30.6	13.701 ± 1.433	Sv	0.309	109
2016 OK1	20	2017-1-3 1:20	2 × 944	1.121	HD11675 (1.102)	60.1	13.784 ± 0.405	Q	0.227	279
2016 PA8	21.9	2016-9-1 6:36	3 × 1200	1.207	SA115-271 (1.155)	3.9	9.712 ± 0.496	Sq	0.243	112
2016 PB8	22.5	2016-8-31 3:49	3 × 1200	1.021	HD202282 (1.032)	10	2.064 ± 0.302	C	0.050	188
2016 PJ66	22.2	2016-9-1 5:09	2 × 1200	1.054	HD202282 (1.032)	8.6	14.037 ± 0.545	Sr	0.266	94
2016 PN38	21.2	2016-8-30 0:21	3 × 1200	1.073	HD202282 (1.038)	30	6.050 ± 0.517	X	0.047	353
2016 PU	21.7	2016-8-30 8:19	2 × 1200	1.093	HD202282 (1.038)	33.3	13.27*0.327	V	0.362	101
2016 QF44	21.4	2016-11-30 3:03	2 × 1500	1.419	Hyades64 (1.446)	6.8	15.31*0.589	Sv	0.309	125
2016 TD18	23.6	2016-11-29 6:36	1 × 900	1.047	HD30947 (1.239)	55.1	10.412*1.255	Sq	0.243	51
2016 UU80	21.1	2016-11-30 6:18	1 × 1500	1.304	Hyades64 (1.446)	32.4	9.638 ± 0.610	Sv	0.309	144
2016 VY5	20.2	2017-1-3 2:00	3 × 630	1.198	HD11675 (1.102)	57.9	17.948 ± 0.300	S	0.211	264
2016 WB8	25.9	2016-11-30 4:26	1 × 1200	1.151	HD20926 (1.062)	29.5	13.013 ± 0.613	L	0.149	23
2016 WG7	26.1	2016-11-29 4:26	1 × 300	1.455	Hyades64 (1.439)	13.9	14.873 ± 0.488	Sq	0.243	16
2016 WJ1	21.3	2016-11-30 4:01	1 × 450	1.378	Hyades64 (1.446)	9.2	10.898 ± 0.311	Sq	0.243	148
2016 WL7	24.3	2016-11-29 2:06	2 × 900	1.111	HD6400 (1.075)	64.3	12.045 ± 0.268	D	0.048	84
2016 WQ	25.5	2016-11-29 1:15	1 × 450	1.077	SA115-271 (1.218)	47.2	9.153 ± 1.014	Q	0.227	22
2016 WZ8	28.4	2016-11-30 4:59	1 × 600	1.458	HD20926 (1.389)	6.4	10.155 ± 0.689	D	0.048	13
2016 YF	25.4	2017-1-2 6:38	2 × 1800	1.129	SA102-1081 (1.142)	57.5	12.254 ± 0.576	S	0.211	24
2016 YM1	22.2	2017-3-1 2:36	2 × 1500	1.225	SA98-978 (1.180)	10.7	4.530 ± 0.524	Cg	0.063	192
2017 BL30	23.3	2017-2-28 1:03	1 × 900	1.233	SA98-978 (1.145)	63.3	14.158 ± 1.287	S	0.211	63
2017 DA36	25.1	2017-2-28 2:19	2 × 800	1.165	SA102-1081 (1.258)	22.9	4.883 ± 0.744	Xk	0.095	41
2017 DA38	25	2017-3-1 5:52	2 × 750	1.415	HD113171 (1.544)	29	15.148 ± 0.296	Sq	0.243	27
2017 DC36	22.1	2017-2-28 3:17	2 × 400	1.087	SA102-1081 (1.258)	20.4	8.361 ± 0.163	S	0.211	110
2017 DL34	25.9	2017-2-28 5:22	2 × 1600	1.147	HD91640 (1.083)	8.9	9.057 ± 0.769	D	0.048	40
2017 DR15	20.9	2017-2-28 4:28	2 × 900	1.386	HD94093 (1.059)	5.8	13.323 ± 0.443	S	0.211	191
2017 DV15	25.1	2017-2-28 7:40	1 × 1500	1.239	SA102-1081 (1.258)	50.2	16.559 ± 0.548	Sv	0.309	23

Notes: The equivalent diameter of each object is computed by taking into account the mean albedo of its assigned taxon (as from Mainzer et al., 2011a), except when an albedo measurement is available in the literature (reported values from: [(1)] Mueller et al., 2011, [(2)] Trilling et al., 2010, [(3)] Mainzer et al., 2014, [(4)] Mainzer et al., 2011b).

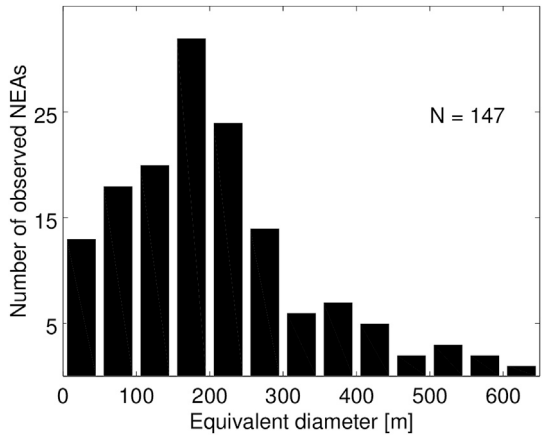

Fig. 1. Distribution of the equivalent diameters of the observed NEAs.

based on visible data only, our findings about A-types have to reckon with some uncertainties due to possible misassignments with respect to other taxa presenting the 1-μm silicate band (we incidentally stress that we find the S-complex asteroids underrepresented in our sample, with respect to larger NEAs, with a deviation of -3.5σ). However, the results seem statistically very robust, also in consideration of the overall good quality of our spectra. The abundance of D-types (4 of which with diameter < 100 m) among our targets looks even more glittering, considering the low albedo of these objects that should disadvantage their detection at the smallest size ranges. Noteworthy, we also outline a relatively high abundance in our sample ($+2.5\sigma$) of featureless X-type NEAs, part of which could be of carbonaceous, primitive nature (see Fornasier et al., 2011, for a review on X-type asteroids). The populations of the rest of the taxa do not differ by more than 2σ with respect to the expected values based on the literature data. The possible implications of an overabundance of organic-rich D-types and olivine-rich A-types among the small NEA population are further discussed in Sec. 4.

3.2. Phase reddening

Phase reddening (i.e., the increasing of the spectral slope with increasing solar phase angle α at the moment of the observation) has been evidenced to affect many bodies of the solar system, from the Moon to Mercury, from Uranus' moons to asteroids (e.g., Schröder et al., 2014, and references therein).

Ideally, to study the phase reddening one should observe each object at different phase angles, and obtain particular coefficients for each asteroid. Of course this would be very much time-demanding if a large population of bodies has to be investigated. However, our observations of NEAs have been performed over a wide range of solar phase angles (~2–94°), allowing us to constrain the "average" phase reddening effect on the visible spectral slope (0.44–0.65 μm; cf. Table 1) for the different taxonomic types. We warn however the reader of the limitations of our approach, as in this way we cannot separate the phase reddening due to the observing geometry from other factors affecting the spectral properties of each asteroid, such as space weathering, particle size effects, etcetera.

The average values of the reddening coefficient γ (e.g., Luu and Jewitt, 1990), defined as the linear fit of the spectral slope vs. phase angle dependence, are given in Table 3 for the most populated compositional groups in our sample (together with the number of objects in each taxon and the measured range of phase angles; again, we used the Octave's *polyfit* routine).

The phase reddening seems to strongly affect moderate-to-high albedo spectral types. The largest phase reddening is seen for olivine-rich A-types (and, to a less extent, Q-types). Asteroids belonging to the S-complex barely show phase reddening, with a large data scatter most probably due to a lower level of composition homogeneity within this taxon (Fig. 5).

Conversely to silicate-rich asteroids, NEAs in the C-complex do not show phase reddening (in particular, disregarding the only point at $\alpha > 50^\circ$ one would obtain $\gamma = -0.010 \pm 0.013$). The visible spectral slopes of the D-types also seem to not increase with the phase angle (disregarding the two reddest D-types, whose spectral slopes are considerably higher than others reported for this class, one would obtain $\gamma = 0.053 \pm 0.027$). In both cases, the data scatter is rather large. The X-complex also shows large dispersions in spectral slopes (probably because of the coexistence in this taxon of objects of either carbonaceous, silicaceous, enstatitic, or metallic nature), although on average a reddening trend could be present (Fig. 6).

4. Discussion and conclusions

Despite of its intrinsic limitations (visible data only; still low statistics), our visible spectroscopic survey of the "small" ($H \geq 20$) near-Earth asteroids reveals some peculiar characteristics of the distribution of taxonomic types within such population, compared to larger bodies.

First of all, we note the relative abundance of olivine-rich A-types (5–10%). Such bodies are very rare among larger NEAs and in the asteroid main belt (where objects of just a few hundred metres in size are not observable). Here we remind the reader of the long-lasting "missing olivine problem" (e.g., Scott et al., 2015, and references therein): decay of ^{26}Al in the early solar system produced a differentiation of the largest accreting planetesimals. Later mutual collisions shattered these early-formed differentiated bodies to produce a much bigger number of smaller asteroids. Several tens of differentiated parent bodies are needed to account for the range of iron meteorite types (coming from the cores of such differentiated bodies) in our collections. However, a differentiated body of chondritic composition should be dominated by the olivine-rich mantle material (~60–80% in mass; Toplis et al., 2013). The apparent shortage of olivine-rich asteroids is a still poorly understood problem in solar system science. At least a dozen of alternative or complementary solutions have been proposed to this missing olivine problem. E.g., Consolmagno et al. (2015) suggested that early differentiated planetesimals may have had non-chondritic bulk compositions, hence not crystallising significant olivine in their mantles, while Elkins-Tanton et al. (2014) proposed that formation of significant olivine was prevented by high viscosity and rapid heat loss in planetesimals. We refer the reader to, e.g., Greenwood et al. (2015), and references therein, for a recent summary about the wide range of possible explanations for such underrepresentation of olivine-rich material that have been proposed. Here we stress that our results may support the "battered to bits" scenario (Burbine et al., 1996): mantle fragments from disrupted differentiated parent bodies could have been shattered to dimensions below a few hundreds of metres, below the limit of detectability of previous spectroscopic surveys. Noteworthy, our findings about the relative abundance of A-types among small asteroids may also strengthen the hypothesis of an exogenous origin for the olivine detected as isolated outcrops on the surface of Vesta (Turrini et al., 2016, and references therein).

In our survey we also found an unexpectedly high number of D-type asteroids, believed to be the most primitive in the solar system. Their very low albedo and featureless red spectra suggest a high abundance of organics and volatiles, which may hold clues regarding the planetary processes that preceded life on Earth (e.g., Hiroi et al., 2001). Indeed, isotopic ratio measurements seem to exclude the hypothesis of a significant contribution of comets to the water of the Earth's oceans and atmosphere, and primitive, carbonaceous asteroids could have played the main role in this regard (Altwegg et al., 2015; Marty et al., 2016). However, D-type asteroids were considered to be very rare in the NEA population. Our results could conversely indicate that they are quite abundant among the small-sized bodies, probably as a consequence of the high fragility of these carbonaceous asteroids, which favors the fragmentation of larger bodies (e.g., Granvik et al., 2016). The robustness of

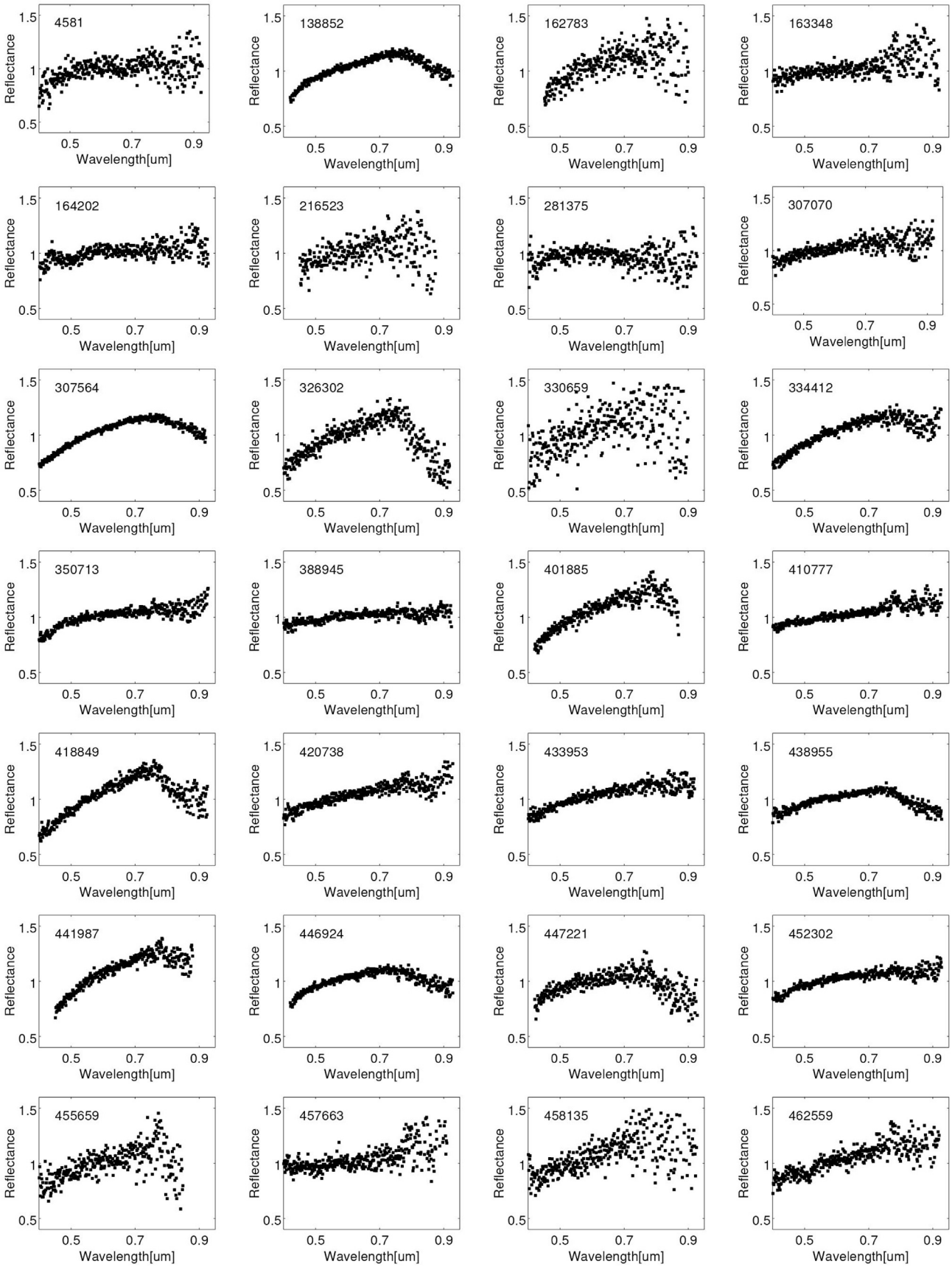

Fig. 2. Obtained reflectance spectra (normalized at 0.55 μm) for 129 NEAs (spectra of further 18 targets are presented in parallel papers, cf. text in Section 2).

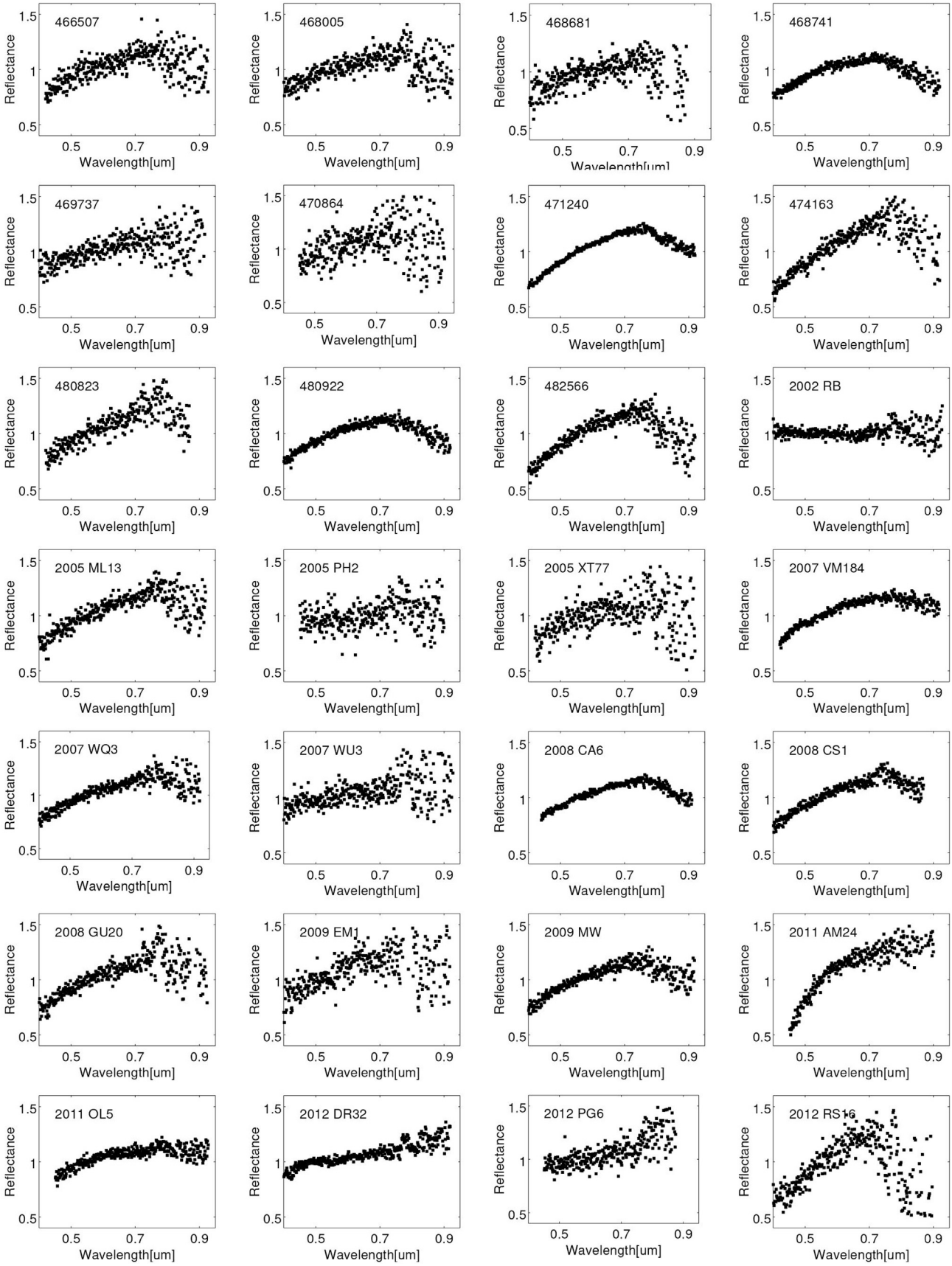

Fig. 2. (*continued*).

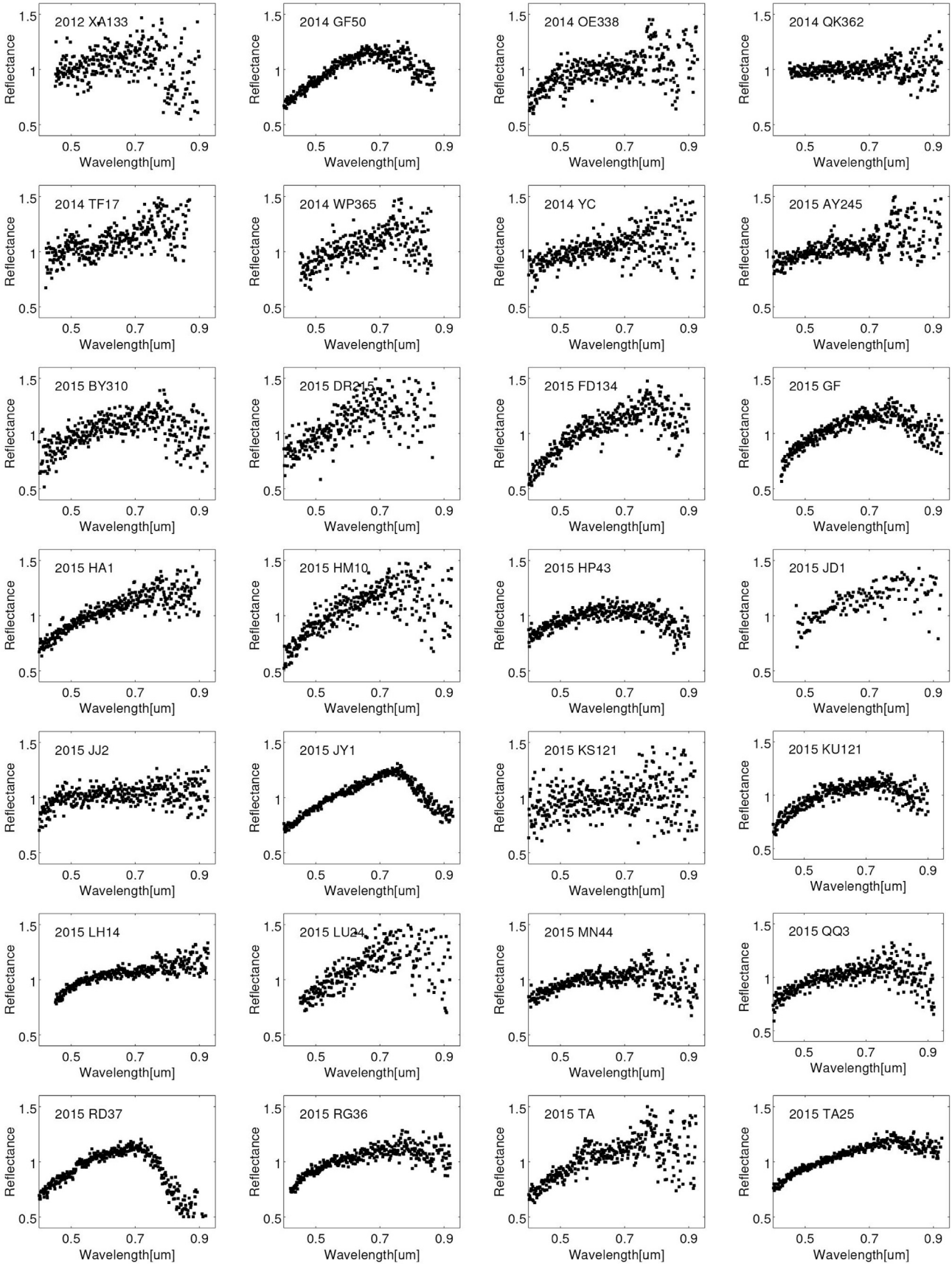

Fig. 2. (*continued*).

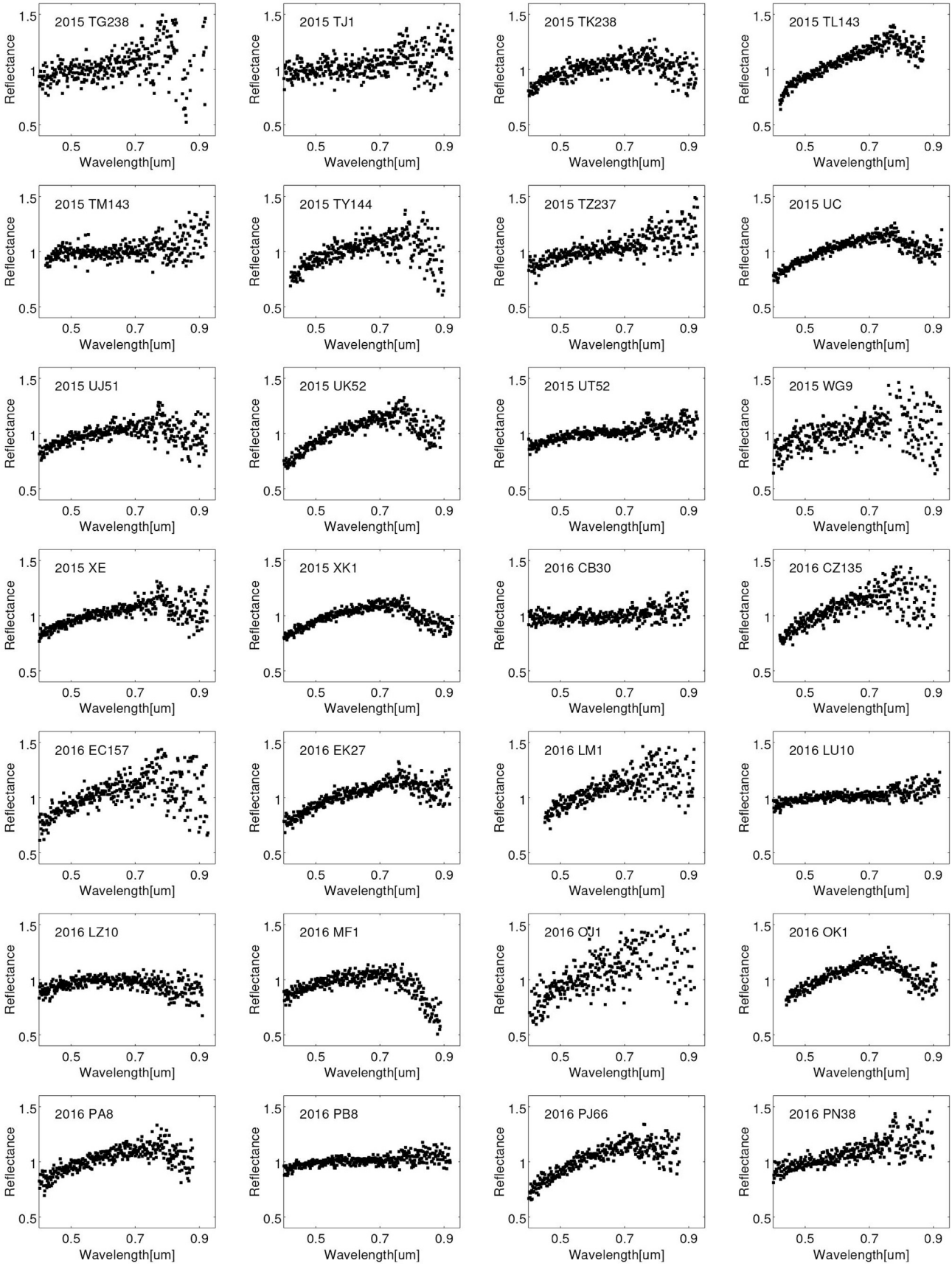

Fig. 2. (*continued*).

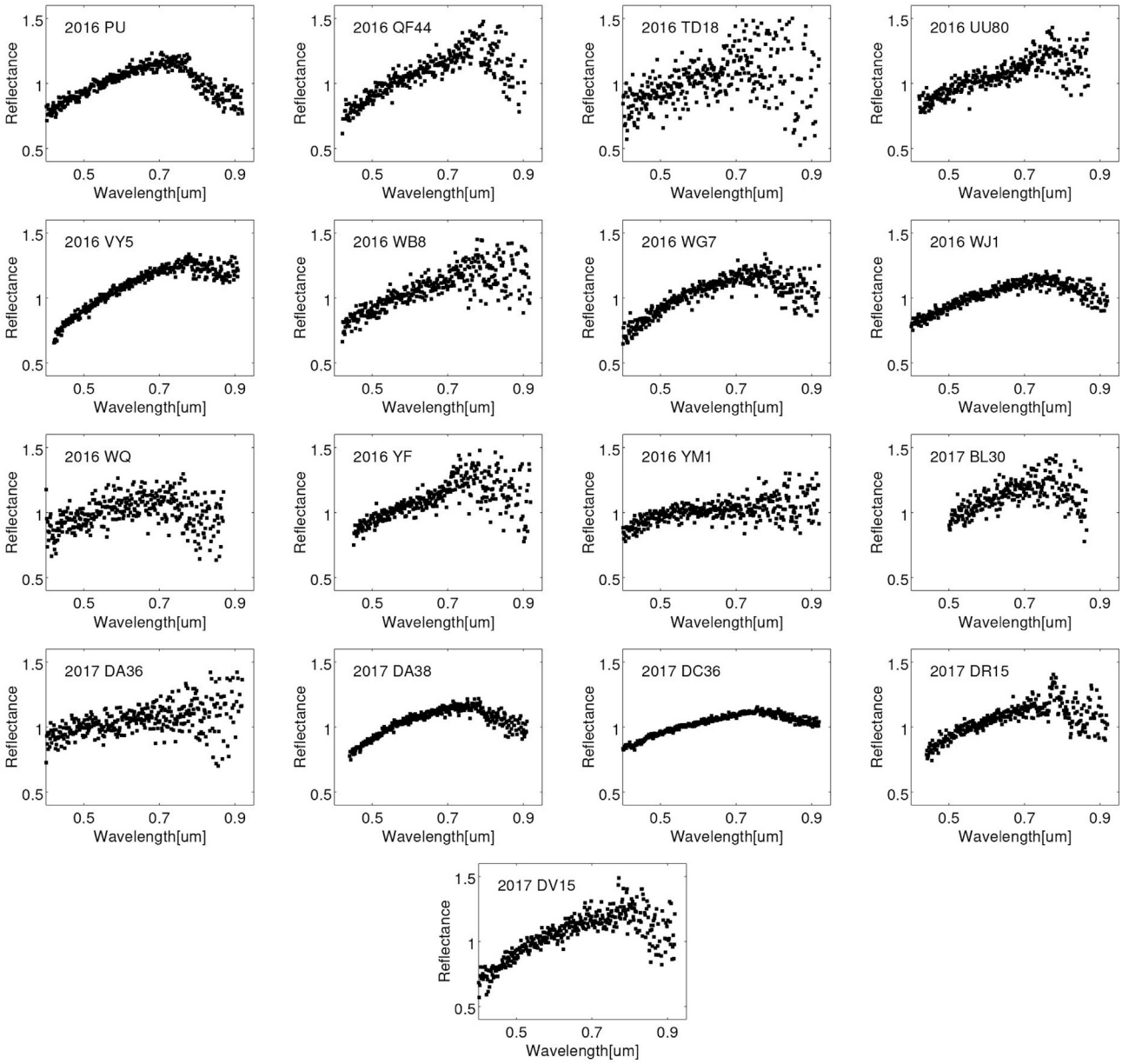

Fig. 2. (*continued*).

this result is outlined by the fact that the very dark D-types should be more difficult to discover/observe at the smallest size ranges. Noteworthy, DeMeo et al. (2014) found a high abundance of D-types among the smallest (<15 km) asteroids in the inner main belt, from which the NEA population is mostly replenished via well-known dynamical paths. Our results hence imply that the asteroidal contribution to the delivery of the prebiotic material to the primitive Earth could be even much more important than foreseen prior of our observations.

Being based on the observation of numerous different targets over a wide range of phase angles, our work also allows us to constrain the spectral phase reddening of asteroids belonging to different compositional/taxonomic groups. On average, we found that low-albedo asteroids (C-complex and D-types) show no/limited phase reddening (confirming and reinforcing the preliminary findings by Lantz et al., 2018), incidentally suggesting a brand new way to discriminate primitive objects within the X-complex, whenever measurements are available spanning a wide range of phase angles. We note however that a quite strong phase reddening (0.104 ± 0.003%/100 nm/deg) has been measured from observations of the nucleus of comet 67P/Churyumov-Gerasimenko by the OSIRIS instrument onboard the ROSETTA mission (Fornasier et al., 2015). The strongest phase reddening is seen for olivine-rich surfaces (A- and Q-types). This is in agreement with previous laboratory results showing that olivine-rich ordinary chondrites are the most affected by phase reddening, though the reason of such behaviour is still unclear (Sanchez et al., 2012). For all of the taxonomic groups, the dependence of the spectral slope by the phase angle is monotonous. We stress that the wavelength dependence of the brightness phase function has always been found monotonous for astronomical observations, with only a few exceptions: those of the martian surface by the Viking 1 lander evidenced a change from reddening to blueing with increasing phase angle, producing an "arch-shaped" phase dependence of the observed spectral slope (Guinness, 1981); moreover, a not-monotonous behaviour is displayed by some observations of the lunar soil (e.g., Shkuratov et al., 2011). Based on laboratory experiments and numerical simulations, Schröder et al. (2014) found a monotonous phase reddening for a microscopically rough regolith, and a non-monotonous arch-shaped

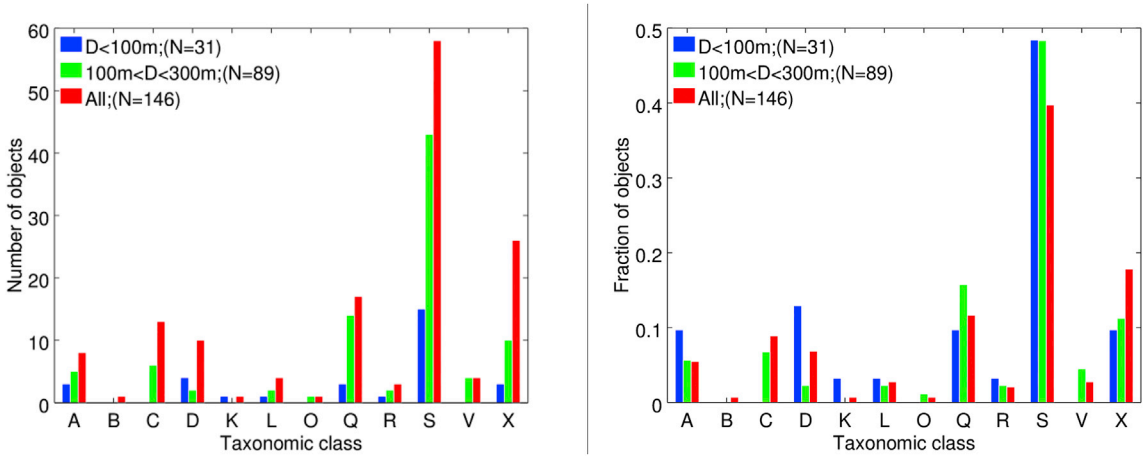

Fig. 3. Taxonomic type distribution of the observed NEAs (left: absolute numbers; right: relative percentages). The distributions for objects smaller than 100 m and for objects in the 100–300 m size bin are shown separately.

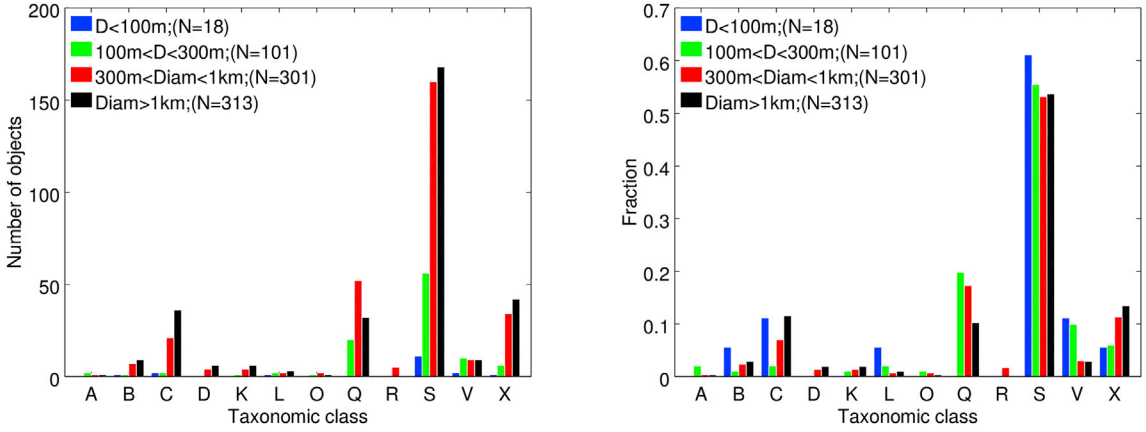

Fig. 4. Taxonomic type distribution of NEAs in the EARN database (left: absolute numbers; right: relative percentages). The distributions for objects with size in the ranges <100 m, 100–300 m, 300–1000 m and >1 km, are shown separately.

Table 2
Statistical comparison between taxonomic distributions of NEAs in our sample and in the literature.

Taxon	A	B	C	D	K	L	O	Q	R	S	V	X
Our sample (%)	5.48 (8/146)	0.68 (1/146)	8.90 (13/146)	6.85 (10/146)	0.68 (1/146)	2.74 (4/146)	0.68 (1/146)	11.64 (17/146)	2.05 (3/146)	39.73 (58/146)	2.74 (4/146)	17.81 (26/146)
146-unit random samples from EARN database (%) [±1σ]	0.47± 0.56	2.45± 1.27	8.38± 2.26	1.38± 0.97	1.49± 0.99	1.09± 0.87	0.54± 0.61	14.23± 2.86	0.68± 0.67	53.94± 4.11	4.10± 1.62	11.25± 2.61
Deviation (σ)	+8.9	−1.4	+0.2	+5.6	−0.8	+1.9	+0.2	−0.9	+2.0	−3.5	−0.8	+2.5

Table 3
Reddening coefficient γ for different spectral types.

Taxon	Phase angle range (deg)	Number of objects	γ (%/100 nm/deg) [0.44–0.65 μm]
A	20–51	8	0.492 ± 0.072
Q	10–80	17	0.074 ± 0.018
S	4–92	58	0.013 ± 0.009
X	5–56	26	0.074 ± 0.021
D	6–64	10	−0.024 ± 0.027
C	2–69	13	−0.032 ± 0.030

behaviour for smooth surfaces. Grynko and Shkuratov (2008), using numerical modelling based on the geometric optics approximation, evidenced a monotonous phase dependence of the spectral slope in the case of single-particle scattering, and non-monotonous behaviour for multiple-component scattering. These authors also found that monotonous phase blueing can happen for particles larger than about 250 μm. Overall, our results hence suggest the presence of a microscopically rough regolith on the surfaces of the observed NEAs, and a similar surface texture for objects belonging to the same compositional group. We remind however that in our approach we averaged out other factors – e.g., peculiar space weathering and particle size – potentially affecting the spectral response of the surfaces of the individual asteroids in each taxon. More dedicated studies of the phase reddening (i.e., with a complete phase coverage for each object) are still needed.

As a concluding remark, we want to emphasize the very important role that the investigation of the "small" near-Earth asteroids can represent for solar system science. The results presented in this paper already provide some clues on different topics related to the formation and early evolution of planetesimals. We should however keep in mind that these results are based on a relatively limited quantity of available

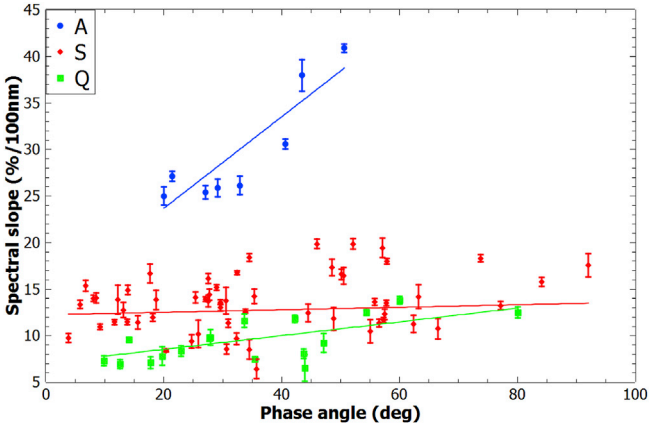

Fig. 5. Spectral slope (0.44–0.65 μm) vs. phase angle for A-, S- and Q-types (blue dots, red diamonds and green squares, respectively). Linear fits are also reported with continuous lines for the three compositional groups (cf. Table 3). (For interpretation of the references to colour in this figure legend, the reader is referred to the Web version of this article.)

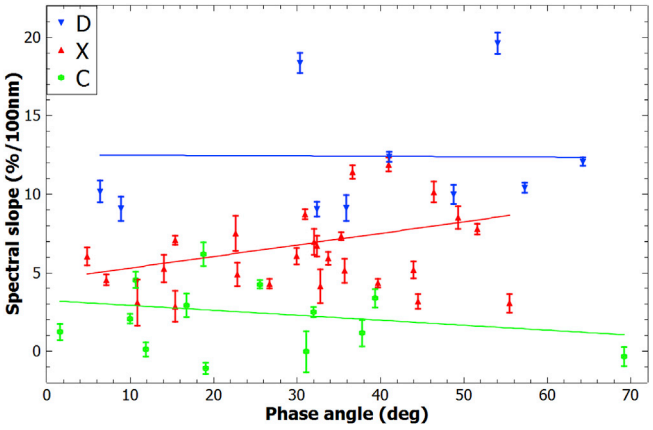

Fig. 6. Spectral slope (0.44–0.65 μm) vs. phase angle for D-, X- and C-types (blue down-triangles, red up-triangles and green dots, respectively). Linear fits are also reported with continuous lines for the three compositional groups (cf. Table 3). (For interpretation of the references to colour in this figure legend, the reader is referred to the Web version of this article.)

data. Future, larger-scale surveys for the systematic physical characterization of newly-discovered NEAs down to the metre-sized (possibly extending to near-infrared wavelengths, to minimize the risk of taxonomic misassignments) will be crucial to further test and extend our findings.

Acknowledgements

This work is based on observations collected at the European Organisation for Astronomical Research in the Southern Hemisphere under ESO programme 095.C-0087. We acknowledge financial support from the NEOShield-2 project, funded by the European Union's Horizon 2020 research and innovation programme (contract No. PROTEC-2-2014-640351). DP has received further funding from the Horizon 2020 programme also under the Marie Skłodowska-Curie grant agreement n. 664931. This project was also supported by the Programme National de Planétologie (PNP) of CNRS/INSU, co-funded by CNES.

References

Altwegg, K., Balsiger, H., Bar-Nun, A., et al., 2015. Science 347, 1261952.
Barucci, M.A., et al., 2018. MNRAS. https://doi.org/10.1093/mnras/sty532.
Binzel, R.P., Rivkin, A.S., Stuart, J.S., et al., 2004. Icarus 170, 259.
Burbine, T.H., Meibom, A., Binzel, R.P., 1996. Meteoritics 31, 607.
Consolmagno, G.J., Golabek, G.J., Turrini, D., et al., 2015. Icarus 254, 190.
Delbo, M., Libourel, G., Wilkerson, J., et al., 2014. Nature 508, 233.
DeMeo, F.E., Binzel, R.P., Slivan, S.M., Bus, S.J., 2009. Icarus 202, 160.
DeMeo, F.E., Binzel, R.P., Carry, B., Polishook, D., Moskovitz, N.A., 2014. Icarus 229, 392.
DeMeo, F.E., Alexander, C.M.O.'D., Walsh, K.J., Chapman, C.R., Binzel, R.P., 2015. In: Michel, P., DeMeo, F.E., Bottke, W.F. (Eds.), Asteroids IV. Univ. of Arizona Press, Tucson, p. 13.
Elkins-Tanton, L.T., Mandler, B.E., Fu, R.R., 2014. In: Conference "Vesta in the Light of Dawn: First Exploration of a Protoplanet in the Asteroid Belt", Abstract #2034.
Fornasier, S., Clark, B.E., Dotto, E., 2011. Icarus 214, 131.
Fornasier, S., Hasselmann, P.H., Barucci, M.A., et al., 2015. A&A 583, A30.
Granvik, M., Morbidelli, A., Jedicke, R., et al., 2016. Nature 530, 303.
Greenwood, R.C., Barrat, J.-A., Scott, E.R.D., et al., 2015. Geochem. Cosmochim. Acta 169, 115.
Grynko, Y., Shkuratov, Y., 2008. In: Kokhanovsky, A. (Ed.), "Light Scattering Reviews 3". Springer-Verlag, Berlin Heidelberg, p. 329.
Guinness, E.A., 1981. J. Geophys. Res. (Solid Earth) 86, 7983.
Hiroi, T., Zolensky, M.E., Pieters, C.M., 2001. Science 293, 2234.
Lantz, C., Binzel, R.P., DeMeo, F.E., 2018. Icarus 302, 10.
Luu, J.X., Jewitt, D.C., 1990. AJ 99, 1985.
Mainzer, A., Grav, T., Masiero, J., et al., 2011a. ApJ 741, 90.
Mainzer, A., Grav, T., Bauer, J., et al., 2011b. ApJ 743, 156.
Mainzer, A., Bauer, J., Grav, T., et al., 2014. ApJ 784, 110.
Marty, B., Avice, G., Sano, Y., et al., 2016. E&PSL 441, 91.
Morbidelli, A., Chambers, J., Lunine, J.I., et al., 2000. M&PS 35, 1309.
Mueller, M., Delbo, M., Hora, J.L., et al., 2011. AJ 141, 109.
O'Brien, D.P., Walsh, K.J., Morbidelli, A., Raymond, S.N., Mandell, A.M., 2014. Icarus 239, 74.
Perna, D., Barucci, M.A., Fulchignoni, M., 2013. A&A Rv 21, 65.
Perna, D., Barucci, M.A., Drube, L., et al., 2015a. P&SS 118, 311.
Perna, D., Kaňuchová, Z., Ieva, S., et al., 2015b. A&A 575, L1.
Perna, D., Dotto, E., Ieva, S., et al., 2016. AJ 151, 11.
Perna, D., Popescu, M., Monteiro, F., et al., 2017. A&A 597, A57.
Pierazzo, E., Chyba, C.F., 1999. M&PS 34, 909.
Popescu, M., Birlan, M., Nedelcu, D.A., 2012. A&A 544, A130.
Popescu, M., et al., 2018. MNRAS. https://doi.org/10.1093/mnras/sty704>.
Reddy, V., Dunn, T.L., Thomas, C.A., Moskovitz, N.A., Burbine, T.H., 2015. In: Michel, P., DeMeo, F.E., Bottke, W.F. (Eds.), Asteroids IV. Univ. of Arizona Press, Tucson, p. 43.
Saladino, R., Botta, G., Delfino, M., Di Mauro, E., 2013. Chem. Eur J. 19, 16916.
Sanchez, J.A., Reddy, V., Nathues, A., et al., 2012. Icarus 220, 36.
Sanchez, J.-P., McInnes, C.R., 2013. In: Badescu, V. (Ed.), Asteroids. Prospective Energy and Material Resources. Springer, Berlin, p. 439.
Schröder, S.E., Grynko, Y., Pommerol, A., et al., 2014. Icarus 239, 201.
Scott, E.R.D., Keil, K., Goldstein, J.I., et al., 2015. In: Michel, P., DeMeo, F.E., Bottke, W.F. (Eds.), Asteroids IV. Univ. of Arizona Press, Tucson, p. 573.
Shkuratov, Y., Kaydash, V., Korokhin, V., et al., 2011. P&SS 59, 1326.
Statler, T.S., Cotto-Figueroa, D., Riethmiller, D.A., Sweeney, K.M., 2013. Icarus 225, 141.
Toplis, M.J., Mizzon, H., Monnereau, M., et al., 2013. M&PS 48, 2300.
Trilling, D.E., Mueller, M., Hora, J.L., et al., 2010. AJ 140, 770.
Turrini, D., Svetsov, V., Consolmagno, G., Sirono, S., Pirani, S., 2016. Icarus 280, 328.